E-ISSN: 2664-6773
P-ISSN: 2664-6765
Impact Factor: RJIF 5.6
IJCBS 2024; 6(2): 42-46
www.chemicaljournal.org
Received: 20-04-2024
Accepted: 26-05-2024

Fouad Warid Mezaal
Ministry of Education, Baghdad Education Directorate, Karkh First, Baghdad, Iraq

Corresponding Author:
Fouad Warid Mezaal
Ministry of Education, Baghdad Education Directorate, Karkh First, Baghdad, Iraq

Utilizing celery extract for green synthesis of iron oxide nanoparticles: Evaluation and anti-GST enzyme activity in *Aedes aegypti* pupae

Fouad Warid Mezaal

DOI: https://doi.org/10.33545/26646765.2024.v6.i2a.101

Abstract
A celery extract was used, and its pH was adjusted, to create iron oxide nanoparticles. Iron oxide nanoparticles were created when celery extract reduced iron (III) chloride ($FeCl_3$). These nanoparticles were then bio-functionalized to serve as stabilizing and capping agents. Iron oxide nanoparticles were generated by UV-visible spectroscopy, scanning electron microscopy (SEM), and X-ray diffraction (XRD). The iron oxide nanoparticles' size, shape, and purity were all significantly impacted by the pH variations. The average crystallite size dropped from 23.23 nm (pH = 1.6) to 20.70 nm (pH = 12), according to the XRD results. The SEM photos show that as the particle size of α-Fe_2O_3 nanoparticles decreased from about 101.60 nm to 34.30 nm, the pH increased as well. Measurements in UV-vis indicate a narrowing of the bandgap from 5.62 and 3.33 eV. When it came to catalytic function, the nanoparticles outperformed the glutathione S-transferase (GST) enzymes in the pupae instar of *Aedes aegypti* mosquitoes, exhibiting a notably higher elimination activity with the highest efficacy. However, when calcined at higher temperatures, the CsPW catalyst was deactived to be less active than the other catalysts after 2-3 cycles. Furthermore, a possible antioxidant content related degradation mechanism of antioxidant was developed from two detected intermediates that is associated ln (Co/C) versus degradation period (h). In the meantime, the death rate of α-Fe_2O_3 nanoparticles at pH 1.6 was 70-75%, while it rose up to 90-99% at pH 12.

Keywords: SEM, XRD, AFM, energy bandgap, glutathione- S-transferase (GST), *Aedes aegypti*

Introduction
Aedes aegypti is a mosquito of medical significance that is linked to the spread of multiple viruses, such as the West Nile virus (WNV), Dengue virus (DENV), Chikungunya virus (CHIKV), Zika virus (ZIKV), and Yellow fever virus (YFV). A small number of visitors to areas where these mosquitoes are endemic have reported several cases. In order to manage patients and devise a plan of action to stop the spread of these viruses, it is crucial to identify them as soon as possible.

Nanotechnology and Green Synthesis
In the modern era, nanotechnology has generated a technology that is widely employed. The study of materials at the atomic or molecular scale and the systems that control them is known as nanotechnology. Nanoparticles are being created by an expanding variety of "green" methods that use safe ingredients. Because it is less expensive, environmentally benign, and does away with the need for dangerous chemicals, high pressure, energy, and temperature, green synthesis is a strong alternative to traditional chemical and physical synthesis methods. Plant extracts replace hazardous reducing chemicals as a combinational reducing and capping agent in the ecologically friendly synthesis of nanoparticles. Nano-scale particles, which are synthesized by green methods, are stabilized in tandem with organic compounds present in plant extracts. In addition, nanoparticles synthesized by plant-mediated pathways are usually low-priced as compared to those by microbial pathways.

Types and Synthesis Routes of Iron Oxide Nanoparticles
The iron oxide nanoparticles can be synthesized in various ways to maintain three main types, including magnetite, maghemite, and hematite. Fe_2O_3 commonly occurs in nature as various mineral forms, which are essentially all noncrystalline Fe_2O_3 but which are always contaminated with oxides of other metals (these are not true Fe_2O_3). The five most prevalent crystalline Fe_2O_3 forms are maghemite, alpha, beta, gamma, and epsilon Fe_2O_3.

The two most prevalent polymorphs of hematite and maghemite minerals are the cubic spinel structure called "gamma" and the hexagonal corundum structure called "alpha."

Overview Fragment: In this work, a more environmentally friendly technique of green synthesis including pH modification that results in energy band gap reduction was used to create iron oxide nanoparticles (IONPs) from celery extract. Iron oxide forms were assessed using X-ray diffraction (XRD). The magnetite nanoparticles' size, shape, and distribution were examined using a scanning electron microscope (SEM). UV-visible spectroscopy was used to determine the absorption spectra of the nanoparticles. Last but not least, anti-GST activity against ESTs of *Aedes aegypti* mosquito pupae instars was observed using a well-diffusion approach.

Material and Methods

Experimental Part Celery leaves were bought from the Serdang city, Malaysia, local market. Iron chloride (99.99%) ($FeCl_3$) was acquired from Sigma-Aldrich, and all other compounds were used exactly as ordered.

Test Subjects

Last-term-instar pupae of *Aedes aegypti* mosquito larvae (weighing 0.18-0.20 g per larva) were obtained from the Department of Zoology UPM University and were used as the test subjects in the present experiments.

Preparation of Celery Extract

After being repeatedly cleaned with distilled water, the celery leaves were dried.

Preparation of Extract

Ten grams of celery leaves were cut and then boiled; compliance with steam distillation in 200 ml distilled water then stirred constantly for 120 min. The mixture was filtered and the resulting extract was used as reducer and cap.

Synthesis of Iron Oxide Nanoparticles (IONPs) Using Celery Extract: For the purpose of creating iron oxide nanoparticles, 125 milliliters of celery extract were dropwise added to a solution containing 0.25 M $FeCl_3$ (4.05 grams in 100 milliliters). The liquid was continuously stirred on a magnetic stirrer for 40 minutes at 70 °C, resulting in a brownish-black coloration from the initial bright yellow hue. After the mixture was moved to a ceramic crucible and heated to 300 °C for two hours in the air, nano-iron oxide powder was produced. Equation (1) depicts the chemical procedure used to create α-Fe_2O_3 nanoparticles.

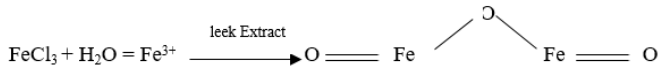

$$FeCl_3 + H_2O = Fe^{3+} \xrightarrow{\text{leek Extract}} O{=}Fe \quad \overset{O}{\diagup\diagdown} \quad Fe{=}O$$

The pH was changed from 1.6 to 12 on a magnetic stirrer using a pH scale, and the effect of the pH on the iron oxide nanoparticles was investigated.

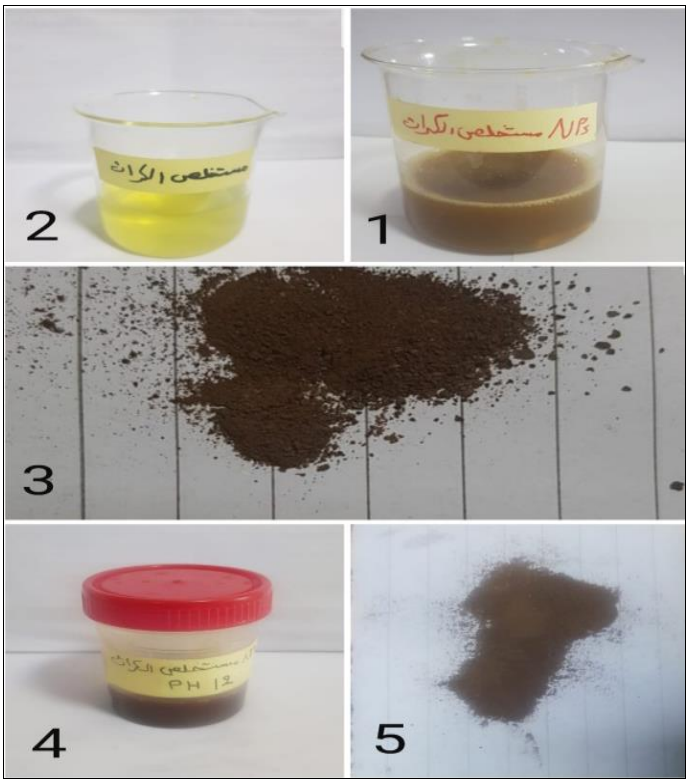

Fig 1: α-Fe_2O_3 nanoparticle synthesis 1. Extract from leeks 2. IONPs at PH of 1.6 3. Pulverized at PH (1.6), 4- When PH (12), IONPs 5-powder at PH of 12

A pH scale with a magnetic stirrer was used to adjust the pH between 1.6 and 12 in order to measure how the pH interacts with the IONPs.

IONPs Characterization

Utilizing more sophisticated methods was a defining characteristic of the IONPs. Phase scan mode was used for X-ray diffractometry. The two angles that were scanned were 30° and 80°. The synthesised IONPs' basic characteristics, including their optical, structural, morphological, elemental structure, and particle size, were examined using a spectrophotometer (UV-1800, Shimadzu).

Anti-GST Activity of IONPs

Herbal functionality of the synthesized IONPs was done by observing the degradation of the GST enzymes in the pupae instar of *Aedes aegypti*. Anti-GST activity of the synthesized α-Fe_2O_3 nanoparticles was analyzed by agar well diffusion

method [9]. *Aedes aegypti*'s pupae instar was used for this assay. With adjustments for control mortality made using the modified Abbott's method, the percentage of the death rate was determined using the equation [10] below: The formula for calculating mortality (%) is \ left (\frac{X - Y}{100 - Y}\right) \times 100}, in where XXX represents the percentage of mortality in the treated sample and YYY represents the percentage of mortality in the control.

Characterization

Figure 2 represents the XRD patterns; for both cases, it confirms that there are crystal planes such as (104), (110), (202), (116), and (122) ensuring that this is hematite (α-Fe2O3) nanoparticles being formed. This has indeed been reported in several previous works [11]. All observed reflection peaks match the expected rhombohedral structure of α-Fe_2O_3. The mean crystallite nano size was close to 23.23 nm while the pH was at 1.6 and about 20.70 nm for pH 12. A higher pH of 12 removes impurities and thus makes it pure. Possibly, this is due to the fact that at higher pH levels, all of the $FeCl_3$ is converted to nano Fe, but at lower pH levels, not all of it is. When comparing pH 1.6 to pH 12, the peak intensities for Fe nanoparticles were higher and more clearly defined at pH 12.

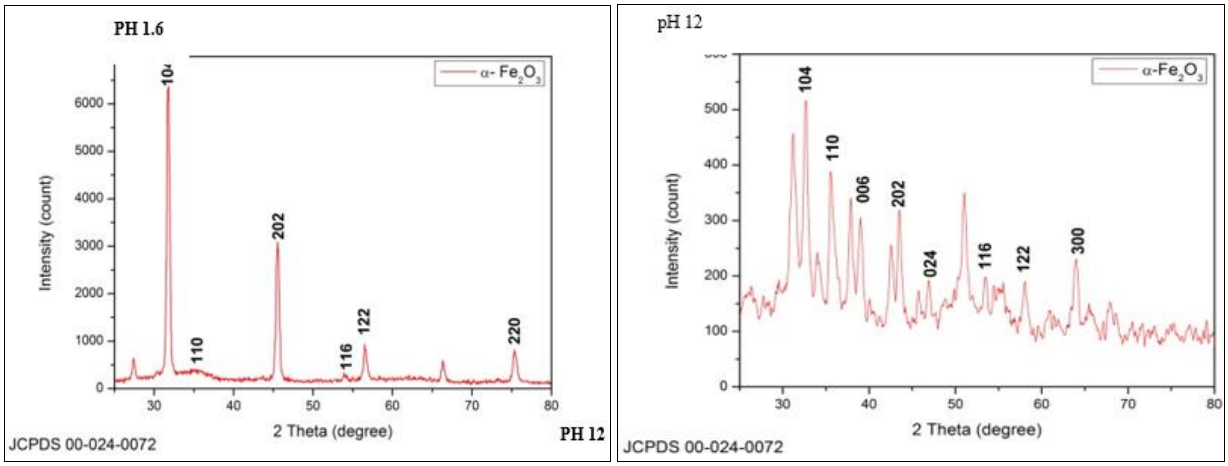

Fig 2: α-Fe_2O_3 nanoparticle XRD data

The particle morphology and size were analyzed using SEM. A micrograph showing rod formations at pH 1.6 is presented in Figure 3(a), where the particle size is 101.60 nm. FE-SEM images of the synthesized α-Fe_2O_3 nanoparticles for pH 12 are depicted in Figure 3(b). The morphology of the particles was changed using the applied experimental parameters, as revealed from the micrograph. Nanoparticles were formed with particle sizes below a micron, about 34.30 nm, as the small particles agglomerated.

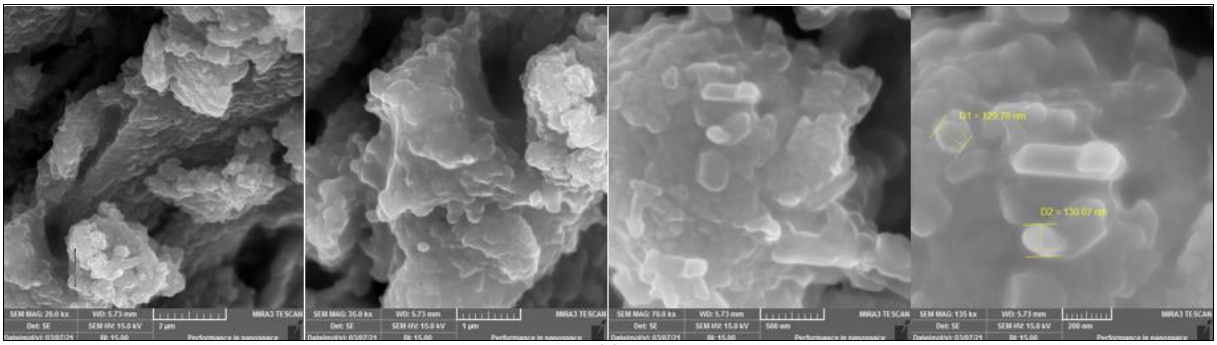

(a)

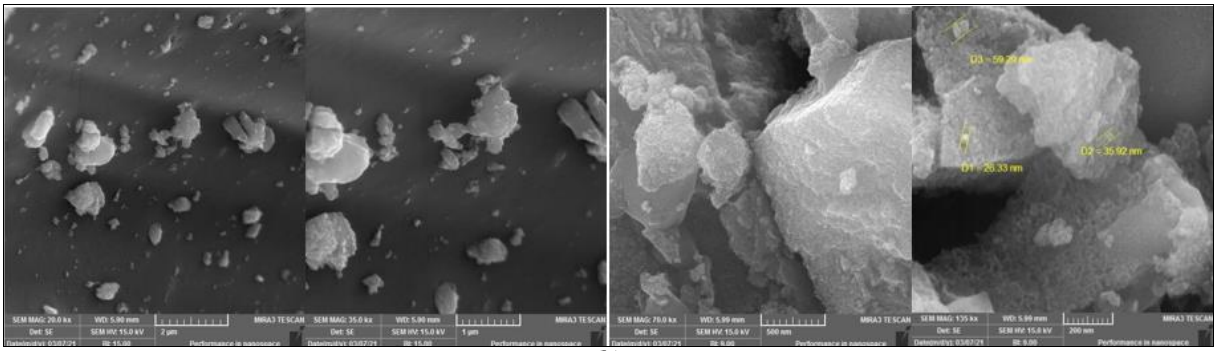

(b)

Fig 3: (a) FESEM image displaying morphology; at PH 1.6 (b) FESEM image displaying morphology; at PH 12

In Figure 4, the energy band gap (Eg) of α-Fe_2O_3 nanoparticles is plotted against the photon energy \(h \nu\) obtained from the plot of the square of the absorption coefficient \((\alpha h \nu)^2\). The plot of the optical band gap of the α-Fe_2O_3 nanoparticle, obtained by extrapolating the straight line at the cross-ratio of energy bands, is 3.33 eV. The

absorbance at 223 nm rises with increasing pH value, reaching its maximum absorbance at pH 12 [12]. Consequently, the energy gap rises with increasing pH; at pH 12, the band gap for α-Fe_2O_3 nanoparticles is 5.62 eV.

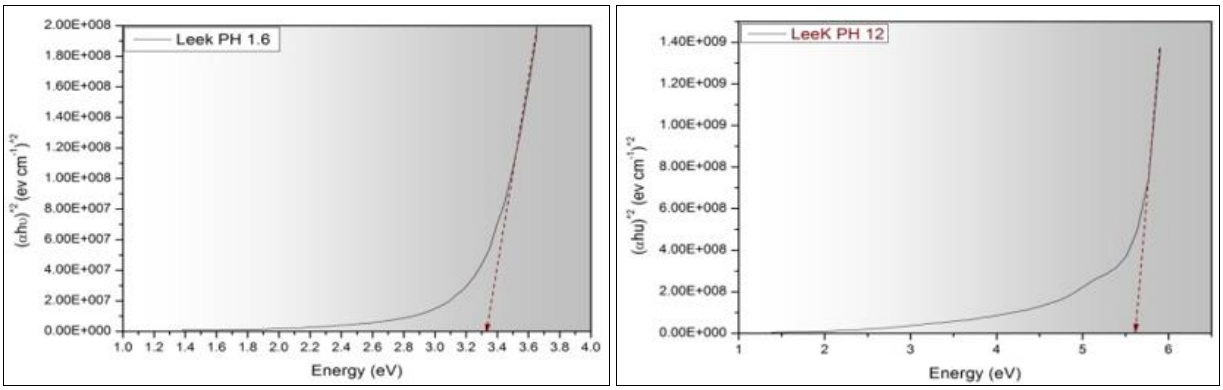

Fig 4: Energy band gap of α-Fe_2O_3 nanoparticles

Anti-GST Activity of α-Fe_2O_3 NPs

The well diffusion method was employed to test the ability of α-Fe_2O_3 nanoparticles to degrade glutathione-S-transferase (GST) enzymes. This technique evaluated the nanoparticles' capacity to break open bacterial cells as well. The phytochemical elements present in plant extracts, along with the nanoparticles, may contribute to anti-GST activity. The test was conducted on terminal-instar pupae of *Aedes aegypti*, weighing between 0.18 and 0.20 grams each. Each of the four groups that the pupae were split into included 107 larvae. Dimethyl sulfoxide (DMSO) or a water-soluble solution could be used for the measurements, as long as the final DMSO content in the assessment wells did not go over 1%. An alternative solvent might be employed, provided that, 72 hours after exposure, its ultimate concentration did not result in more than 10% mortality. It is advised to examine a variety of concentrations at least five distinct levels in order to get accurate results. The accompanying figure shows the specific steps involved in this examination.

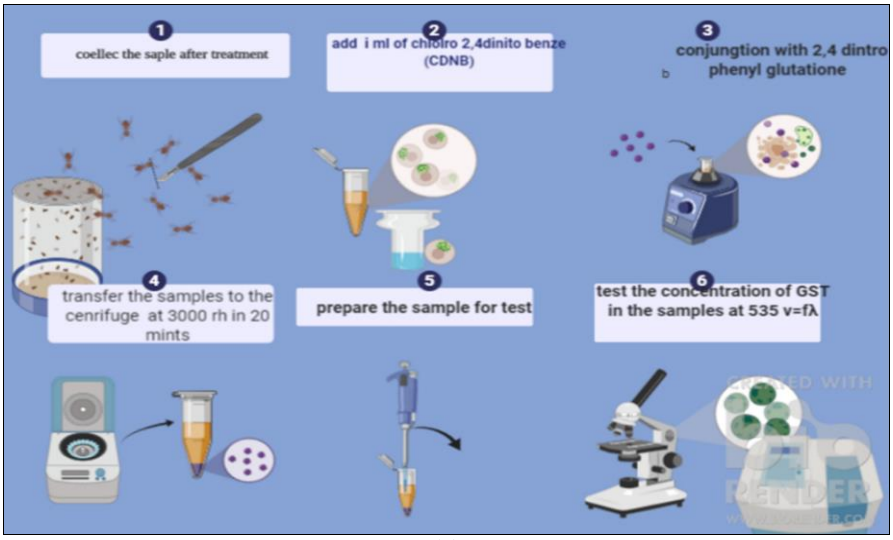

(a)

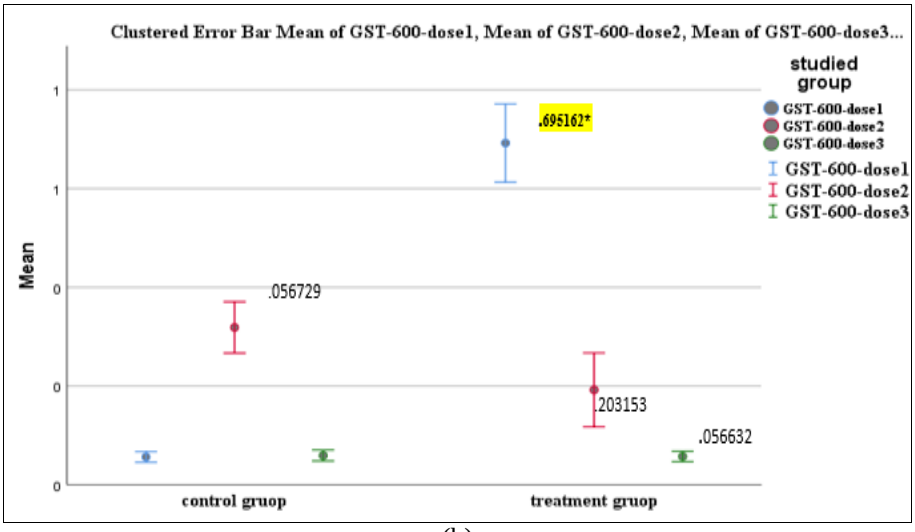

(b)

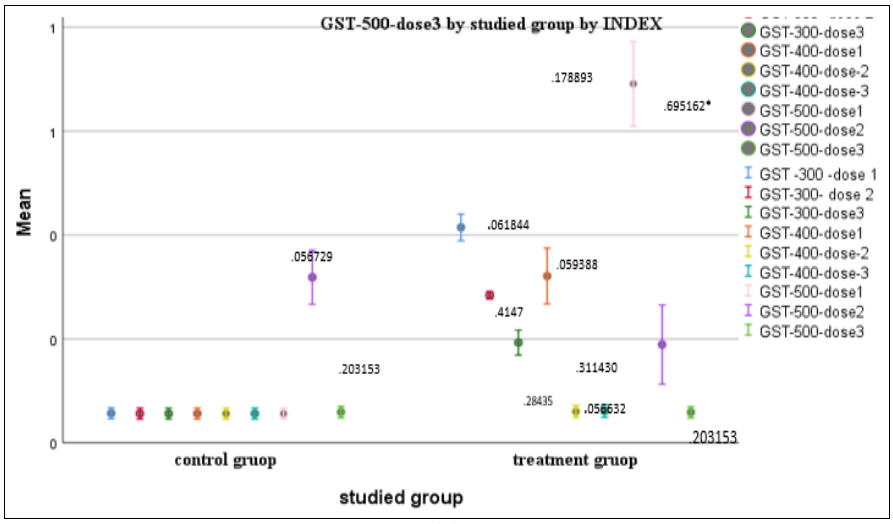

(c)

Fig 5: (a) The method used to measure the activity of glutathione-S-transferase (GST). (b) GST-300 concentration comparison by dosage. (c) A comparison of the treatment and control groups

A noteworthy distinction in GST levels between the groups under investigation is depicted in Figure 5(b). There was a noticeable variation in the initial concentration of titanium nanoparticles that were calcined at 300 degrees Celsius and catalyzed by nitrogen. This discovery is consistent with other research that emphasizes the immune system's maintenance and the activation of antioxidant system responses in reaction to chemicals, harmful radiation, and oxidative stress brought on by free radicals. The study discovered that the concentration of antioxidants starts to decline as the exposure time exceeds 24 to 36 hours and the focus ratio rises. Grasp the biochemical reactions of the organisms being studied requires a grasp of this pattern. Furthermore, Figure 5(c) highlights the notable distinctions between the *Aedes aegypti* pupae exposed to nanoscale radiation treatment group and the control group, highlighting the effects of such treatments on biological systems.

Conclusion

Using a straightforward chemical process, celery (Apium graveolens) extract and $FeCl_3$ were combined to create iron oxide nanoparticles (IONPs) that were then heated to 300°C for two hours. According to XRD data, the average crystallite size dropped from 23.23 nm to 20.70 nm when the pH was raised to 12. According to SEM pictures, at pH 1.6, the particle size of α-Fe_2O_3 NPs was around 101.60 nm, and as pH increased, it decreased to 34.30 nm. The energy band gap increased from 3.33 eV to 5.62 eV, according to UV-vis measurements. *Aedes aegypti* pupae were used to test the iron oxide nanoparticles' anti-GST properties. At pH 1.6, the death rate of α-Fe_2O_3 NPs ranged from 80-90%, and at pH 12, it rose to 90-95%. Glutathione-S-Transferase (GST) enzymes were efficiently destroyed by iron oxide nanoparticles synthesized from celery extract containing $FeCl_3$. However, the photocatalytic activity was greatly decreased during calcining at a higher temperature. Based on the link between ln (Co/C) and degradation time (h), a potential mechanism involving the concentration of exposure dose and the duration of nanocomposite exposure was proposed for the degradation of antioxidant material. This study presents a novel method for the production, characteristics, and use of iron oxide nanoparticles, emphasizing their efficiency in the photodegradation of GST enzymes in *Aedes aegypti* pupae instars.

References

1. Kostaropoulos I, Papadopoulos AI, Metaxakis A, Boukouvala E, Papadopoulou-Mourkidou E. Glutathione S-transferase in the defence against pyrethroids in insects. Insect Biochem Mol. Biol. 2001;31(4-5):313-319.
2. Fatimah I. Green synthesis of silver nanoparticles using extract of Parkia speciosa Hassk pods assisted by microwave irradiation. J Adv Res. 2016;7(6):961-969.
3. Kavitha K, *et al*. Plants as green source towards synthesis of nanoparticles. Int Res J Biol Sci. 2013;2(6):66-76.
4. Philip D. Rapid green synthesis of spherical gold nanoparticles using *Mangifera indica* leaf. Spectrochim Acta A Mol. Biomol. Spectrosc. 2010;77(4):807-810.
5. Prem AA. Green synthesis and characterization of iron oxide nanoparticles using *Phyllanthus niruri* extract. Orient J Chem. 2018;34(5):2583-2589.
6. Bhuiyan MSH, *et al*. Green synthesis of iron oxide nanoparticle using Carica papaya leaf extract: Application for photocatalytic degradation of remazol yellow RR dye and antibacterial activity. Heliyon, 2020, 6(8).
7. Nagajyothi P, *et al*. Green synthesis of iron oxide nanoparticles and their catalytic and *in vitro* anticancer activities. J Clust. Sci. 2017;28(1):245-257.
8. Demirezen DA, *et al*. Green synthesis and characterization of iron oxide nanoparticles using Ficus carica (common fig) dried fruit extract. J Biosci. Bioeng. 2019;127(2):241-5.
9. Vujtek M, *et al*. Ultrafine particles of iron (III) oxides by view of AFM-Novel route for study of polymorphism in nano-world. Sci. Technol. Educ. Microsc. 2003;1(8):1-8.
10. Kanagasubbulakshmi S, Kadirvelu K. Green synthesis of iron oxide nanoparticles using Lagenaria siceraria and evaluation of its antimicrobial activity. Def. Life Sci. J. 2017;2(4):422-427.
11. Salem DM, Ismail MM, Aly-Eldeen MA. Biogenic synthesis and antimicrobial potency of iron oxide (Fe_3O_4) nanoparticles using algae harvested from the Mediterranean Sea, Egypt. Egypt J Aquat. Res. 2019;45(3):197-204.
12. Bouafia A, Laouini SE. Green synthesis of iron oxide nanoparticles by aqueous leaves extract of *Mentha pulegium* L.: effect of ferric chloride concentration on the type of product. Mater Lett. 2020;265:127364.